SEASONAL AND INTERANNUAL VARIABILITY IN CO_2 SNOWFALL WITHIN THE MARTIAN NORTH POLAR VORTEX

N. R. Alsaeed, **P. O. Hayne**, **V. Concepcion**, *Laboratory for Atmospheric and Space Physics, University of Colorado, Boulder, USA (noora.alsaeed@colorado.edu)*

Introduction: The polar regions on Mars play an important role in the thermal regulation and circulation of the atmosphere. In the winter, strong westerly jets isolate the cold air above the poles from lower latitudes. This aptly named polar vortex inhibits transport of dust and other condensates into the poles [1,2]. Temperatures within the polar vortex boundary drop to the freezing point of carbon dioxide, allowing it to condense out both directly onto the surface and as snowfall [3]. As it is the main constituent of the Martian atmosphere, the surface-atmosphere exchange of CO_2 is one of the fundamental processes in both the present and past climate on Mars, mainly due to its ability to significantly alter the atmospheric pressure and heat balance of the planet on seasonal and orbital timescales [4,5]. It is therefore important to understand what forces affect the dynamics of the polar vortex and subsequently the atmospheric processes such as snowfall that occur within it.

In this work we use atmospheric retrievals of temperature and CO_2 ice cloud opacity from the Mars Climate Sounder (MCS) on board NASA's Mars Reconnaissance Orbiter (MRO) to analyze patterns in the winter polar vortex and CO_2 ice clouds over the north pole for Mars years (MY) 29 to 34. We also couple the MCS data with a simple snowfall model to determine precipitation rates of CO_2 snow and analyze patterns in the amounts and distribution of snowfall.

Data and Methods: We use data from MCS, an infrared radiometer that measures the thermal emission of the atmosphere to retrieve vertical profiles of temperature, dust, water vapor and other condensates [6]. In this work we use retrievals of the pressure, temperature, and dust opacities [7] which are converted to CO_2 ice opacities as described in [8]. We limit the data to the northern polar winter between L_S = 180° and 360° with latitudes above 65 N for MY 29 to 34. For each L_S in each year, we convert the CO_2 opacities to CO_2 density profiles, and use different binning procedures in latitude and longitude to parse out patterns in the data.

In our analysis of the polar vortex, we bin the temperature between 10 and 20 km above the surface into 5-degree latitude and longitude bins for each L_S and define the vortex boundary at T = 170 K. We do this for the entirety of northern winter for all Mars years between MY 29 and 34 and observe changes in the area covered by the polar vortex over seasonal and annual timescales. Results are shown in figures 1 and 2.

For the snowfall analysis, we input the CO_2 profiles into a snowfall model to track deposition onto the surface. The snowfall model we use is a cloud settling model described by a Fokker-Planck-Smoluchowski diffusion equation which incorporates both diffusion and gravitational settling of the ice particles [9]. We aggregate the snowfall amounts over the entire winter season for each Mars year.

Results: In our analysis, four main patterns emerge: 1) There is strong coupling between dust activity in the southern hemisphere and polar vortex dynamics in the northern polar winter. 2) The stable polar vortex tends towards an elliptical wave 2 shape. 3) Snowfall rates vary with dust activity from both localized and global dust storms. 4) There is a persistent longitudinal stationary wave in CO_2 ice cloud densities within the polar vortex.

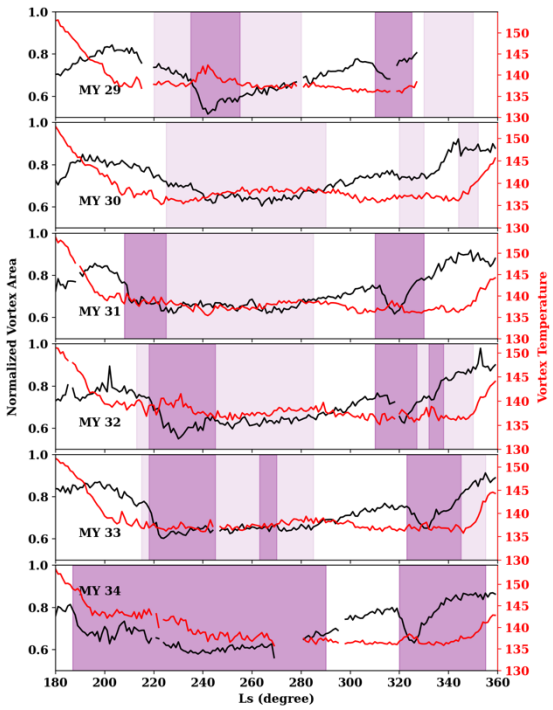

Figure 1: Northern polar vortex area (black) and mean temperature (red) for MY 29 to 34. The light purple shaded areas correspond to weaker dust events where the dust opacity (scaled to 610 Pa) was larger than 0.25, and darker purple areas correspond to stronger dust events where the dust opacity was larger than 0.375. The polar vortex boundary is defined to be at T = 170 K. The area is given as a fraction of the total area encompassed above 50 N. Dust information was sourced from the Mars Climate Database [10].

Discussion:

Polar vortex coupling with dust activity. Unlike the polar vortex on Earth, which grows during the winter season, the northern polar vortex on Mars shrinks in size multiple times throughout the winter [2]. As described in previous work [11, 12], this shrinking is due to the presence of a dust cycle on Mars. Figure 1 shows the strong coupling between dust events in the southern hemisphere and the shrinking of the polar vortex in the northern pole. We observe that the reduction in size of the polar vortex is also coupled with warmer temperatures within the vortex, and enhanced snowfall as shown in figure 4.

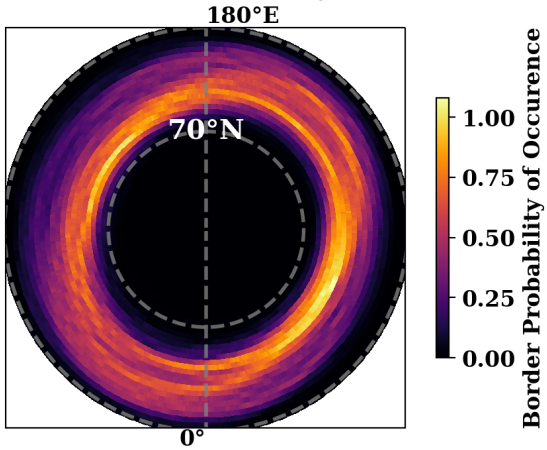

Figure 2: Shape of the north polar vortex given by the boundary lines between MY 29 to 33. The boundaries were found by taking the temperature contour at T = 170 K for each L_S, over-plotted with a normalized color bar.

Elliptical wave 2 shape is most stable. The north polar vortex on Mars displays a unique characteristic wave 2 shape. This shape has been observed and modeled before and is likely driven by topography in the polar region [1,2]. It is characterized by an ellipticity of roughly 0.5, with the semi-major axis pointing in the direction of 150 E. We find that this elliptical shape is disrupted during strong dust storms when the vortex shrinks in size. We believe this disruption may be a driving factor in the variation of snowfall discussed in the next section.

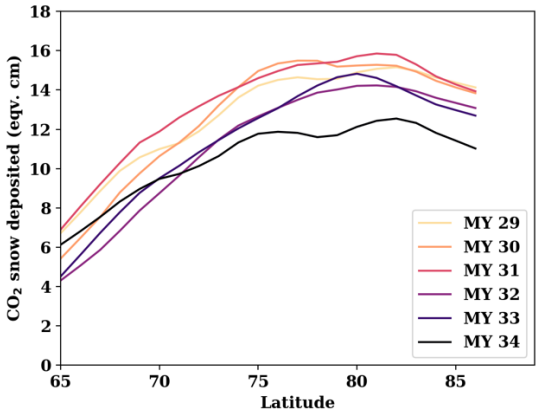

Figure 3: Total CO_2 snowfall deposited onto the northern polar surface at the end of winter as a function of latitude.

Snowfall variability with dust activity. Our results show active snowfall throughout the entirety of the northern winter season, with slight year to year variation in the total amounts of snowfall as shown in table 1 and figure 3. We find that there is significant and measurable interannual variability in the snowfall, with most snowfall occurring in MY 29 followed by a gradual decline. This is of note as it follows the planet-encircling dust storm of MY 28.

Table 1: Total CO_2 ice deposition due to snowfall at the end of northern winter.

Mars Year	CO_2 ice mass deposited (kg)	CO_2 ice equivalent thickness (cm)
29	1.23e15	13
30	1.18e15	13
31	1.25e15	13
32	1.03e15	11
33	1.05e15	11
34	1.02e15	11

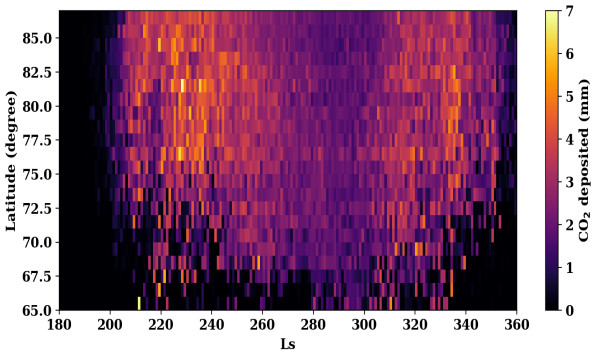

Figure 4: CO_2 snowfall deposition per latitude onto the northern polar surface as a function of L_S. Plotted values are the median deposition for MY 29 to 33.

Within each winter season, figure 4 shows clear enhancement in the amount of snowfall around L_S 220° and at L_S 320°, timeframes that align with the categorized B and C dust storms that kick off in the south [13]. This may indicate that smaller dust storms enhance snowfall by allowing more dust to be injected into the polar vortex area at its boundary which serve as condensation nuclei for ice to precipitate out. However, when parsing it out by year, not every dust storm enhances snowfall. The more likely scenario is that the dust storms introduce instabilities within the polar vortex which can create localized pockets of cooler/warmer air that could affect CO_2 condensation either way.

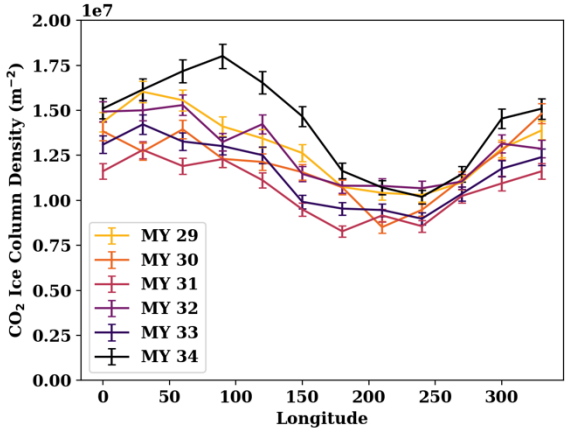

Figure 5: Winter CO_2 ice cloud column densities as a function of longitude. The column densities span 10 to 60 km above the polar surface and are averaged over 80° – 90° N for the entire winter season L_S 180° – 360° of each year.

Longitudinal stationary wave. Within the polar vortex region, a clear longitudinal wave pattern emerges in the density of the CO_2 clouds, as seen in figure 5. This pattern is persistent from one Mars year to the next and enhances during the global dust storm in MY 34. The stationary planetary wave is likely a forced oscillation driven by topography [14], which possibly affects the ellipticity of the vortex as well [2].

Acknowledgements: Part of this work was supported by NASA through the MRO project and by the United Arab Emirates Mohammed bin Rashid Space Center through support for N. R. Alsaeed.

References: [1] Waugh, D. W., et al. (2016) *JGR: Planets* 121(9) 1770-1785. [2] Mitchell, D. M., et. al. *JRMS*, *141*(687), 550-562. [3] Forget, F., and Pollack, J. B. (1996). *JGR*, *101*(E7), 16865-16879. [4] Leighton, R. B., & Murray, B. C. (1966), Science, 153(3732), 136-144. [5] Pollack, J. B., et al. (1990), *JGR*, 95(B2), 1447-1473. [6] McCleese, D. J., et. al. (2007), *JGR*, 112(E5). [7] Kleinböhl, A., et al. (2009), *JGR*, 114(E10). [8] Gary-Bicas, C. E., et. al. (2020). *JGR*, 125(5). [9] Hayne, P. O., et al. (2014), *Icarus*, 231, 122-130. [10] Millour, E., et. al. (2018), *From Mars Express to ExoMars*, 68. [11] Wilson, R. J. (1997). *GRL*, *24*(2), 123-126. [12] Guzewich, S. D., et. al. (2016). *Icarus*, *278*, 100-118. [13] Kass, D. M., et. al. (2016). *GRL*, *43*(12), 6111-6118. [14] Banfield, D., et. al. (2003). *Icarus*, *161*(2), 319-345.